Taylor & Francis
Taylor & Francis Group

Combustion Science and Technology

ISSN: (Print) (Online) Journal homepage: https://www.tandfonline.com/loi/gcst20

Aerodynamics of Tsuji Burners with Augmented Fuel Injection

Brandon Li, José Graña-Otero, Antonio L. Sánchez & Forman A. Williams

To cite this article: Brandon Li, José Graña-Otero, Antonio L. Sánchez & Forman A. Williams (2022): Aerodynamics of Tsuji Burners with Augmented Fuel Injection, Combustion Science and Technology, DOI: 10.1080/00102202.2022.2041613

To link to this article: https://doi.org/10.1080/00102202.2022.2041613

COMBUSTION SCIENCE AND TECHNOLOGY
https://doi.org/10.1080/00102202.2022.2041613

Taylor & Francis
Taylor & Francis Group

Aerodynamics of Tsuji Burners with Augmented Fuel Injection

Brandon Li, José Graña-Otero, Antonio L. Sánchez, and Forman A. Williams

Department of Mechanical and Aerospace Engineering, University of California San Diego, La Jolla, California, USA

ABSTRACT

Tsuji burners, in which flames may be anchored in the forward stagnation region of a cylindrical porous fuel injector placed in a uniform air stream, are addressed here for moderately large Reynolds numbers. Attention is focused on conditions under which the fuel-injection velocity is not sufficiently small compared with the outer air velocity for the boundary layer to remain attached to the forward part of the cylinder surface. In the resulting flow, the flame is embedded in the thin mixing layer that forms at the surface separating the outer air stream from the fuel stream, both having, in general, different densities. The flow on the air side of the mixing layer is potential, while that on the fuel side usually is rotational because exit conditions for the fuel injection generate vorticity, for example, by imposing a requirement that the fuel must emerge normal to the cylinder surface, which is the condition analyzed herein. It is shown that introduction of a suitably density-weighted stream function reduces the problem to that of constant-density flow, with the density-square-root-weighted ratio of injection velocity to free-stream velocity Λ emerging as the only controlling parameter. The numerical solution, involving determination of the vorticity distribution in the inviscid fuel flow through an iterative scheme, provides the structure of the flow, including the mixing-layer location and the inviscid-flow strain rate there. Numerical results are presented for values of Λ ranging from small ($\Lambda \ll 1$) to large ($\Lambda \gg 1$) injection velocities. The inviscid results in the limit of vanishingly small injection velocities (Λ approaching zero) demonstrate that, unlike the prediction of the potential-flow solution, when the fuel-side flow is rotational the outer air velocity never approaches the classical solution corresponding to potential flow around a solid cylinder ($\Lambda = 0$), a result affecting the interpretation of analyses of experiments involving flames stabilized on Tsuji burners as the boundary layer is blown off. In particular, with rotational fuel-side flow, the streamline separating the fuel and oxidizer regions lies farther from the cylinder surface, resulting in a larger near-quiescent wake and a lower strain rate along the separating streamline.

ARTICLE HISTORY
Received 11 September 2021
Revised 19 November 2021
Accepted 8 December 2021

KEYWORDS
Counterflow flames;
Nonpremixed combustion;
Tsuji burners

Introduction

Tsuji burners have been used to investigate laminar counterflow flames for over 50 years (Tsuji and Yamaoka 1967). As indicated in the schematic diagram shown on the left-hand side of Figure 1, the flame is established in the forward stagnation-point region of a porous cylinder of radius a placed in a uniform air stream of velocity U_∞, with the fuel released by

CONTACT Antonio L. Sánchez als@ucsd.edu Department of Mechanical and Aerospace Engineering, University of California San Diego, La Jolla, California 92093–0411, USA

injection perpendicular to the cylinder surface with velocity U_i. Although the precise direction of fuel injection may depend on details of construction of the porous cylinder, outlet fuel-flow channels typically are considered to be narrow enough to force approximately normal exit flow. In most applications, the Reynolds number $Re = \rho_A U_\infty a/\mu_A$ (based on the density ρ_A and viscosity μ_A of the air stream) is large although not large enough for the laminar flow to become unsteady near the cylinder surface, and the injection velocity U_i is small, of order $U_i \sim U_\infty/Re^{1/2}$, so that the streamline separating the external airflow from the fuel flow lies in the near-wall boundary layer of characteristic thickness $\delta = a/Re^{1/2} \ll a$ that develops over the forward side of the cylinder. Effects of molecular transport are confined to this boundary layer, where the fuel and the air mix and react, while the flow outside is nearly inviscid. The reacting boundary layer, containing the flame, displays a self-similar structure near the forward stagnation point, determined by the local value of the strain rate exerted by the outer flow. The flame continues developing along the cylinder wall away from the stagnation region, until separation eventually occurs.

In analyzing the flame that develops near the forward stagnation point, it is customarily assumed (Tsuji 1982) that the azimuthal velocity component on the outer edge of the boundary layer corresponds to that of the potential-flow solution obtained by superposition of a doublet and a uniform stream, an approximation that is known to be reasonably accurate for configurations without fluid injection at the cylinder surface; see, e.g., Batchelor (2000). Correspondingly, the value of the strain rate at the forward stagnation point, which determines the local self-similar solution there, is simply given by $2U_\infty/a$. Effects of likely departures from this widely used approximation are to be investigated as part of our analysis.

The flow structure depicted on the left-hand side of Figure 1, corresponding to injection velocities $U_i \sim U_\infty/Re^{1/2} \ll U_\infty$, changes drastically when the fuel is injected with velocities that are comparable to U_∞, displacing the stagnation point to distances of order a away

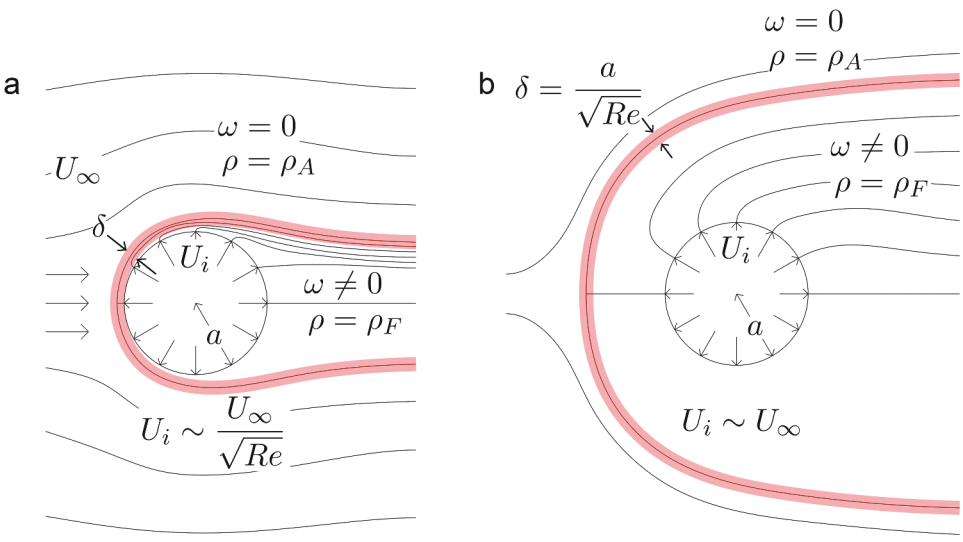

Figure 1. A schematic view of the flow field in Tsuji burners with $U_i \sim U_\infty/Re^{1/2}$ (left plot) and with $U_i \sim U_\infty$ (right plot). The shaded region represents the thin layer where air and fuel mix.

from the cylinder surface, as shown on the right-hand side of Figure 1. For $Re \gg 1$, mixing and reaction occur only in a thin mixing layer of characteristic thickness $\delta = a/Re^{1/2} \ll a$ localized at the fluid interface separating the incoming airflow from the injected fuel gas. At leading order in the limit $Re \gg 1$ the reacting mixing layer emerges as a free surface separating two regions of inviscid flow, as indicated in Figure 1. The outer flow is potential, because the air stream carries no vorticity, but the inner flow generally is rotational, because the injected fuel stream has vorticity, as needed for the injection velocity to be normal to the cylinder surface, for example, the situation addressed here for the first time. It is worth pointing out that the inviscid structure investigated here, involving a potential region and a rotational region, is reminiscent of that found in idealized nonplanar premixed flames, where vorticity production results from the flame deflection associated with the density jump across the reaction front (Zel'dovich et al, 1980). As discussed by Squires and Libby (1994), the flow description, involving jump conditions at the flame, is a challenging task that necessitates specific numerical methods accounting for the free-boundary character of the problem.

The Tsuji-burner analysis is formulated first for general order-unity values of the Reynolds number Re. Consideration of the limit $Re \gg 1$ will be seen to reduce the problem to that of inviscid flow, with the solution depending on two parameters, namely, the fuel-to-air density ratio ρ_F/ρ_A and the fuel-to-air velocity ratio U_i/U_∞. Use of a proper density-weighted vorticity/stream-function formulation (Carpio et al, 2017; Weiss, Coenen, Sánchez 2017) further reduces the problem to one of constant-density flow, with $\Lambda = (\rho_F/\rho_A)^{1/2} U_i/U_\infty$ entering as the only governing parameter. The solution involves determination of the vorticity distribution on the cylinder surface, which is computed numerically for different values of Λ. The solution provides the location of the forward stagnation point and the associated local value of the strain rate, relevant to determining the structure and extinction of a flame that may be located in the mixing layer surrounding the dividing streamline. Analyses of flame structures in such mixing layers have been reviewed by Linán and Williams (1993a). The shape of the streamline separating the two reactant streams and the streamwise variation of the velocity profiles will also be obtained.

Formulation of the problem

The porous-burner configuration investigated here is shown in Figure 2. The cylinder radius a and external air velocity U_∞ will be used to scale the length coordinates and time in the problem, yielding dimensionless cylindrical coordinates (r, θ) and corresponding velocity components $\mathbf{v} = (v_r, v_\theta)$. Following standard convention, the azimuthal angle θ is to be measured counterclockwise from the horizontal rightward ray, with the uniform airflow approaching from $\theta = \pi$. Because of the existing symmetry, it suffices to give the solution in the half plane $0 \leq \theta \leq \pi$.

General formulation for $Re \sim 1$

The air density ρ_A and temperature T_A will be used to define a dimensionless density ρ and a dimensionless temperature T. Similarly, the transport properties of the air stream will be used to define a dimensionless viscosity μ, thermal conductivity k, and molecular diffusivity

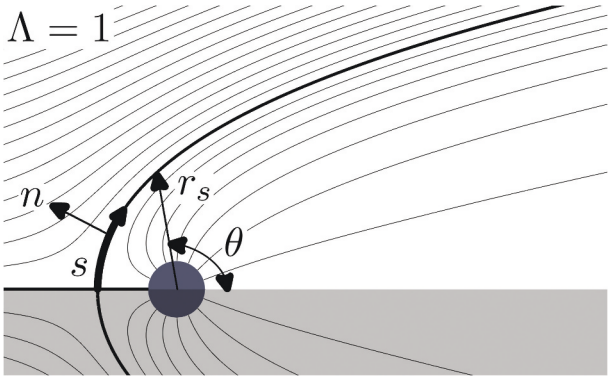

Figure 2. Illustration of the flow configuration, with indication of relevant coordinates; the streamlines shown correspond to $\Lambda = 1$.

D_i of species i. Buoyancy forces are neglected in the analysis, an appropriate simplification for small combustors with sufficiently large Froude numbers $U_\infty^2/(ga) \gg 1$. For the low-Mach-number conditions prevailing in applications, the steady form of the conservation equations (given, e.g., in Williams 1985) for a reacting gas mixture with constant specific heat c_p reduce to

$$\cdot(\rho\mathbf{v}) = 0 \tag{1}$$

$$\rho\mathbf{v}\cdot \quad \mathbf{v} = - \quad p + \frac{1}{Re} \quad \cdot[\mu(\quad \mathbf{v} + \quad \mathbf{v}^T)] \tag{2}$$

$$\rho\mathbf{v}\cdot \quad T = \frac{1}{PrRe} \quad \cdot(k \quad T) - \sum_N \frac{m_i}{(\rho_A U_\infty/a)} \frac{h_i}{(c_p T_A)}, \tag{3}$$

$$\rho\mathbf{v}\cdot \quad Y_i = \frac{1}{Sc_i Re} \quad \cdot(\rho D_i \quad Y_i) + \frac{m_i}{\rho_A U_\infty/a}, \tag{4}$$

where p represents the spatial pressure differences scaled with $\rho_A U_\infty^2$, Pr is the Prandtl number, and Y_i, h_i, and Sc_i denote the mass fraction, enthalpy of formation, and Schmidt number of species i. The rate of production of mass of chemical species i, $\dot{m}_i$, identically zero in the feed streams, must be evaluated for a given chemistry description in terms of the local values of T and Y_i. These differential equations must be supplemented with expressions for the temperature and composition dependences of the dimensionless transport coefficients k, μ, and D_i and with the equation of state, written in the low-Mach-number form

$$\rho T \sum_i (Y_i W_A/W_i) = 1, \tag{5}$$

with W_i and W_A denoting, respectively, the molecular mass of species i and the mean molecular mass of the air stream. To integrate the above differential equations, it is necessary to specify the temperature and composition of the air stream as $r \to \infty$ and of the fuel stream at $r = 1$, as well as the corresponding boundary velocity distributions, which are given by

$$\begin{cases} (v_r, v_\theta) \to (\cos\theta, \sin\theta) & \text{as} \quad r \to \infty \\ (v_r, v_\theta) \to (U_i/U_\infty, 0) & \text{at} \quad r = 1 \end{cases} . \tag{6}$$

The limit $Re \gg 1$

In the inviscid limit $Re \gg 1$, molecular transport becomes negligible in (2)–(4). In the absence of mixing, the chemical reaction cannot proceed, so that (3) and (4) reduce to $\mathbf{v} \cdot \quad T = \mathbf{v} \cdot \quad Y_i = 0$, indicating that the temperature and composition of the steady flow, and therefore also the density according to (5), remain constant along streamlines. As a result, there exists a fluid interface, $r = r_s(\theta)$, separating an external region with density $\rho = 1$ from an internal region with density $\rho = \rho_F/\rho_A$. This separating interface $r = r_s(\theta)$ is a tangential discontinuity, with the velocity on the outer and inner sides satisfying

$$|\mathbf{v}^+|^2 = (\rho_F/\rho_A)|\mathbf{v}^-|^2, \tag{7}$$

as follows from conservation of head along the boundary streamlines, with the superscripts $+$ and $-$ denoting conditions along the limiting streamlines in the air and fuel regions at $r = r_s^+$ and $r = r_s^-$, respectively.

The problem can be formulated conveniently in terms of the stream function ψ, defined such that

$$v_r = \frac{1}{r}\frac{\partial \psi}{\partial \theta} \quad \text{and} \quad v_\theta = -\frac{\partial \psi}{\partial r}, \tag{8}$$

which serves to satisfy (1) automatically. For the planar flow investigated here, the vorticity

$$\omega = \frac{1}{r}\frac{\partial}{\partial r}(r v_\theta) - \frac{1}{r^2}\frac{\partial v_r}{\partial \theta} \tag{9}$$

satisfies

$$v_r \frac{\partial \omega}{\partial r} + \frac{v_\theta}{r}\frac{\partial \omega}{\partial \theta} = 0, \tag{10}$$

as can be seen by taking the curl of the inviscid form of (2). Eq. (10) reveals that the vorticity is conserved along streamlines, so that $\omega = \omega(\psi)$. Use of (8) in (9) provides

$$\frac{1}{r}\frac{\partial}{\partial r}\left(r\frac{\partial \psi}{\partial r}\right) + \frac{1}{r^2}\frac{\partial^2 \psi}{\partial \theta^2} = -\omega(\psi), \tag{11}$$

as a Poisson equation for ψ with an unknown nonlinear source function $\omega(\psi)$. The boundary conditions needed for integrating (11) reduce to

$$\begin{cases} \psi - (U_i/U_\infty)(\theta - \pi) = \partial\psi/\partial r = 0 & \text{at } r = 1 & \text{for } 0 \le \theta \le \pi \\ \psi = 0 & \text{at } \theta = \pi & \text{for } 1 \le r < \infty \\ \psi \to r\sin\theta & \text{as } r \to \infty & \text{for } 0 < \theta \le \pi \\ \psi = -\pi(U_i/U_\infty) & \text{at } \theta = 0 & \text{for } 1 \le r < \infty \end{cases} \tag{12}$$

when account is taken of the symmetry present in the problem. In (12), the arbitrary value of ψ along $r = r_s(\theta)$ has been selected to be $\psi = 0$, with the air/fuel sides corresponding to positive/negative values of ψ, respectively. The separating surface $r = r_s(\theta)$ is an unknown free boundary to be determined with use made of the additional boundary condition (7) written in the form

$$\left[\left(\frac{\partial\psi}{\partial r}\right)^2 + \frac{1}{r^2}\left(\frac{\partial\psi}{\partial\theta}\right)^2\right]^+ = \left(\frac{\rho_F}{\rho_A}\right)\left[\left(\frac{\partial\psi}{\partial r}\right)^2 + \frac{1}{r^2}\left(\frac{\partial\psi}{\partial\theta}\right)^2\right]^- \quad \text{at} \quad \psi = 0. \tag{13}$$

The function $\omega(\psi)$ is related to the unknown distribution of vorticity on the cylinder wall $\omega_w(\theta)$ through

$$\omega = \begin{cases} 0 & \text{for } \psi \geq 0 \\ \omega_w[(U_\infty/U_i)\psi + \pi] & \text{for } -\pi(U_i/U_\infty) \leq \psi \leq 0 \end{cases}. \tag{14}$$

Reduction to a problem with equal densities

The free-boundary problem defined in (11)–(14) determines $\psi(r, \theta)$ along with the vorticity distribution $\omega_w(\theta)$ and the separating surface $r_s(\theta)$ for given values of U_i/U_∞ and ρ_F/ρ_A. As shown previously (Carpio et al, 2017; Weiss, Coenen, Sánchez 2017), the solution can be simplified by incorporating a renormalization factor $(\rho_F/\rho_A)^{1/2}$ in the definition of new kinematic variables

$$\hat{\omega} = (\rho_F/\rho_A)^{1/2}\omega \quad \text{and} \quad \hat{\psi} = \begin{cases} \psi & \text{for } \psi > 0 \\ (\rho_F/\rho_A)^{1/2}\psi & \text{for } \psi < 0 \end{cases}. \tag{15}$$

The problem then reduces to the integration of

$$\frac{1}{r}\frac{\partial}{\partial r}\left(r\frac{\partial\hat{\psi}}{\partial r}\right) + \frac{1}{r^2}\frac{\partial^2\hat{\psi}}{\partial\theta^2} = -\hat{\omega}(\hat{\psi}). \tag{16}$$

with boundary conditions

$$\begin{cases} \hat{\psi} - \Lambda(\theta - \pi) = \partial\hat{\psi}/\partial r = 0 & \text{at } r = 1 & \text{for } 0 \leq \theta \leq \pi \\ \hat{\psi} = 0 & \text{at } \theta = \pi & \text{for } 1 \leq r < \infty \\ \hat{\psi} \to r\sin\theta & \text{as } r \to \infty & \text{for } 0 < \theta \leq \pi \\ \hat{\psi} = -\pi\Lambda & \text{at } \theta = 0 & \text{for } 1 \leq r < \infty, \end{cases} \tag{17}$$

and the additional condition that the rescaled vorticity and its distribution on the cylinder surface $\hat{\omega}_w(\theta)$ are related by

$$\hat{\omega} = \begin{cases} 0 & \text{for } \hat{\psi} \geq 0 \\ \hat{\omega}_w(\psi/\Lambda + \pi) & \text{for } -\pi\Lambda \leq \hat{\psi} \leq 0. \end{cases} \tag{18}$$

The dynamic condition (13) is automatically satisfied when written for the renormalized variables, thereby removing the need to consider the separating surface $r_s(\theta)$ as a free boundary, a greatly helpful simplification. It is seen that the reduced formulation depends only on the single governing parameter

$$\Lambda = \left(\frac{\rho_F}{\rho_A}\right)^{1/2} \frac{U_i}{U_\infty}, \tag{19}$$

the square root of the ratio of the dynamic pressure of the fuel feed stream to that of the incoming air stream for normal fuel injection, which may have been expected for this inviscid flow. The streamlines depicted in Figure 2 correspond to $\Lambda = 1$.

The solution to the problem defined above determines $\hat{\psi}(r, \theta)$ as well as the vorticity distribution on the cylinder surface $\hat{\omega}_w(\theta)$. The latter is ultimately determined by the condition that the fuel is injected perpendicular to the wall, in that there is a single distribution $\hat{\omega}_w(\theta)$ for which $\partial\hat{\psi}/\partial r = 0$ at $r = 1$. If, instead, the fuel were injected with zero vorticity, then the stream function would be given by the potential-flow solution, a simple superposition of a doublet and source at the origin on a uniform flow,

$$\hat{\psi}_p = (r - 1/r)\sin\theta + \Lambda(\theta - \pi), \tag{20}$$

which exhibits a nonzero azimuthal velocity $-\partial\hat{\psi}/\partial r = -2\sin\theta$ on the cylinder surface. This potential-flow solution, which neglects the presence of vorticity on the fuel side of the flame imposed by cylinder exit configurations that force no velocity components tangential to the cylinder surface, is to be compared with the complete inviscid solution determined by numerical integration of (16)–(18). Although experimental measurements of near-cylinder velocity fields with blown-off cylinder boundary layers are not available, it seems likely that they would be closer to those obtained from the present analysis than those for potential flow.

Computational results

The problem defined in (16)–(18) was solved numerically using the iterative scheme described in the Appendix. Results were obtained for injection conditions corresponding to values of Λ in the range $0.1 \leq \Lambda \leq 10$. Selected illustrative results are presented in Figures 3–6. The boundary streamline $r_s(\theta)$ is indicated in Figure 3 by a thicker line, which, for potential fuel-side flow, is

$$r_s = \sqrt{1 + \left[\frac{(\pi - \theta)\Lambda}{2\sin\theta}\right]^2} + \frac{(\pi - \theta)\Lambda}{2\sin\theta}. \tag{21}$$

Explicit formulas such as this are not available for rotational flows, which require numerical integration.

As may be seen in Figure 3, for large values of Λ, the forward stagnation point is about twice as far upstream for the rotational flow than it is for the potential flow, the direction of this difference being understandable in view of the suppression of the downstream-directed azimuthal velocity components at the surface of the cylinder by the boundary conditions applies there for the rotational flow. The differences between the rotational-flow and potential-flow solutions are, however, found to be greatest for small injection velocities, $\Lambda \ll 1$, where the amount of vorticity needed at injection to satisfy the condition of zero tangential velocity is very large; as Λ decreases, the normal component of the injection velocity decreases, but the tangential component

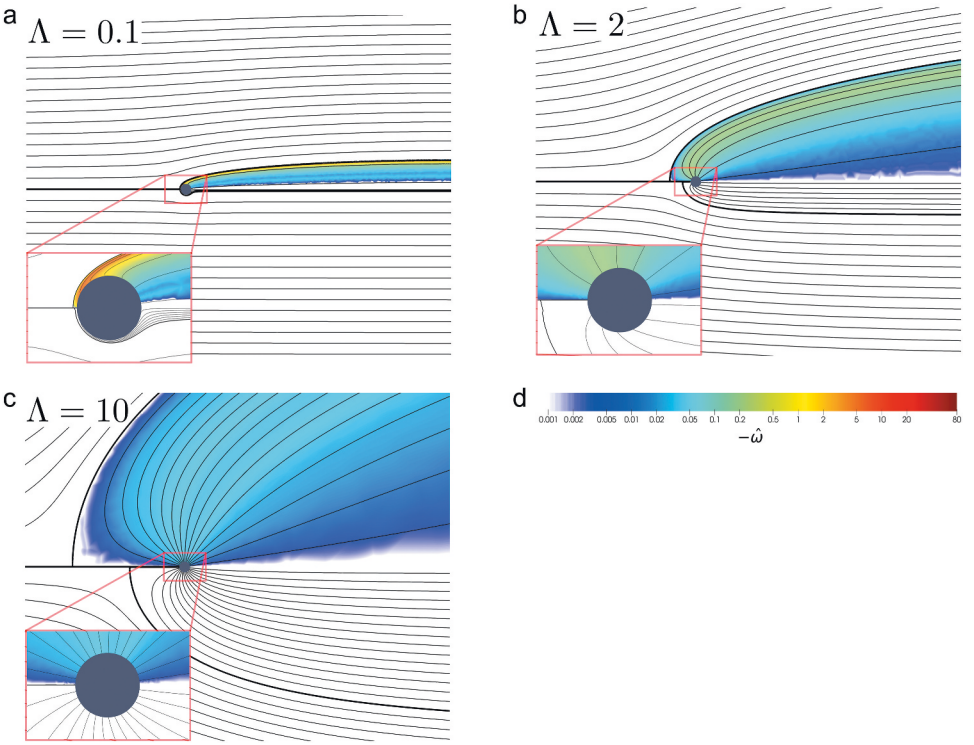

Figure 3. The upper half of each panel represents the streamlines and vorticity distribution corresponding to different values of Λ obtained by integration of (16) with boundary conditions (A2). The lower half shows the streamlines of the corresponding potential flow, evaluated with use made of (20). The spacing used for the stream function is $\delta\hat{\psi} = 2$ on the air side $\hat{\psi} > 0$ and $\delta\hat{\psi} = (0.1, 1, 2)$ for $\Lambda = (0.1, 2, 10)$ on the fuel side $\hat{\psi} < 0$, except for the inset corresponding to $\Lambda = 0.1$, which uses $\delta\hat{\psi} = 0.05$.

remains unchanged to provide a potential flow, so that the difference between the tangential and normal velocity components increases with decreasing Λ for the potential flow, thereby leading to the requisite greater decrease in the tangential velocity component of the rotational flow, compared with that of the potential flow, resulting in the increase in vorticity of the rotational flow with decreasing Λ. In the plot in Figure 3 for the small injection velocity, the boundary streamline of the potential-flow solution remains at distances of order $r_s - 1 \sim \Lambda$ from the cylinder surface, but when the vorticity is present the boundary streamline is farther away, and a region of high vorticity separates from the surface at $\theta \simeq 3\pi/4$ and evolves downstream to produce a comparatively massive wake with vanishing fluid motion, markedly different from that encountered in the potential-flow solution.

An explicit quantification of the vorticity generated in the fuel-injection process is given in Figure 4. As explained above, the amount of vorticity decreases with increasing injection velocities. To further quantify this effect, use can be made of the potential-flow solution (20) to evaluate the tangential-to-normal velocity ratio on the cylinder surface, yielding $2 \sin\theta/\Lambda$. Since this ratio is inversely proportional to Λ, becoming infinite as Λ approaches zero, the local *spin* needed to deflect the injection

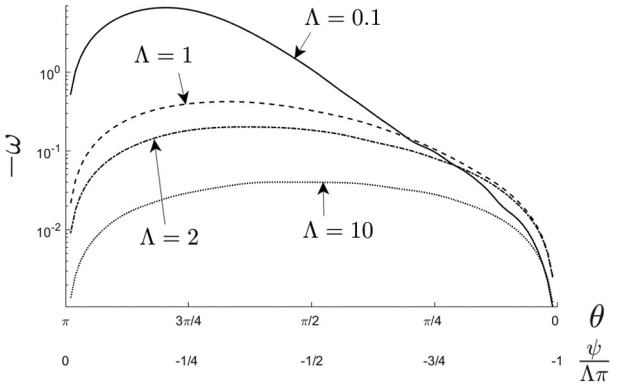

Figure 4. The function $\omega(\psi) = \omega_w(\theta)$ for selected values of Λ.

velocity to a direction normal to the surface is smaller for larger Λ. The vorticity maximum on the surface for $\Lambda = 0.1$, about ten times that for $\Lambda = 1$, occurs, consistent with the results shown in Figure 3, approximately at $\theta \simeq 3\pi/4$, upstream from the midpoint where it resides for larger values of Λ, causing the relative bulging of the low-velocity wake to be smaller. The asymmetry of the vorticity distribution on the surface understandably decreases with increasing injection velocity.

Figure 5 shows the stagnation-point radial location $r_s(\pi)$ and the associated strain rate $\hat{A}_o$, which can be evaluated from the local value of $-r_s^{-1}\partial^2\hat{\psi}/\partial r\partial\theta$ and would be relevant for analyzing flames stabilized in this stagnation region. For the potential-flow solution,

$$r_s(\pi) = \sqrt{1 + (\Lambda/2)^2} + \Lambda/2, \tag{22}$$

and the corresponding stagnation-point strain rate is

$$\hat{A}_o = -\frac{1}{r}\frac{\partial^2\hat{\psi}_p}{\partial r\partial\theta} = \frac{r_s^2(\pi) + 1}{r_s^3(\pi)}. \tag{23}$$

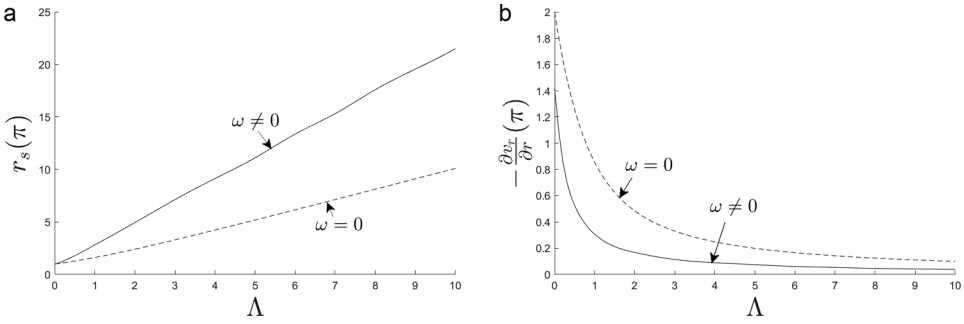

Figure 5. The radial location of the stagnation point and corresponding strain rate obtained by integration of (16) (solid curves) and from evaluation of the potential-flow stream-function expressions (20) (dashed curves).

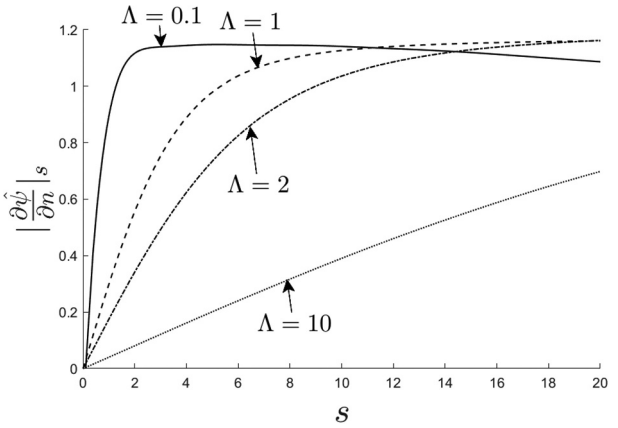

Figure 6. The distribution of velocity along the separating streamline $\psi = 0$ for selected values of Λ.

The comparison in the figure indicates that the strain rate for the potential-flow solution is appreciably larger than that for rotational flow for all values of Λ, with relative differences becoming greater for increasing injection velocities. At small injection velocities $\Lambda \ll 1$, the strain rate computed numerically approaches a limiting value $\hat{A}_o \simeq 1.35$, markedly different from the potential-flow prediction $\hat{A}_o = 2$.

As indicated in the introduction, in the limit $Re \gg 1$, mixing and reaction are confined to the mixing layer that separates the two streams. The structure and extinction of a flame in the mixing layer can be analyzed using as local coordinates the distance s measured along the dividing streamlines $r_s(\theta)$ and the associated transverse coordinate n, both indicated in Figure 2. The velocities on the air and fuel side of the mixing layer satisfy (7). The corresponding equations for the strained mixing layer, given for instance in Linán and Williams (1993b), depend on the outer flow through the local value of the strain rate, which can be computed from the streamwise variation of the velocity on the air and fuel sides of the separating streamline $\partial|\mathbf{v}^+|/\partial s$ and $\partial|\mathbf{v}^-|/\partial s$, where $|\mathbf{v}^+| = |\partial\hat{\psi}/\partial n|_s$ and $|\mathbf{v}^-| = |\partial\hat{\psi}/\partial n|_s(\rho_A/\rho_F)^{1/2}$, with $|\partial\hat{\psi}/\partial n|_s$ denoting the magnitude of the gradient of $\hat{\psi}$ at $r_s(\theta)$. In view of this application, the variation of the velocity $|\partial\hat{\psi}/\partial n|_s$ with s is shown in Figure 6. As previously anticipated, the largest slope is found at $s = 0$, corresponding to the forward stagnation point, where the flame would be subject to the highest strain rate. The gradient at the stagnation point is largest at the smallest values of Λ, as is to be expected from the smaller effective cylinder radius at lower fuel-injection rates, whence flame extinction may be achieved by decreasing Λ, that is, either by increasing the air velocity or by decreasing the fuel flow rate.

Conclusions

When the fuel injection in Tsuji burners is strong enough to blow the boundary layer away from the cylinder surface, analysis in the limit $Re \gg 1$ reveals two inviscid regions separated by a mixing layer, an air region having potential flow and a fuel region where the flow is quite liable to be rotational. A formulation for describing the flow in these two regions has been derived that reduces the flow to one dependent on only a single parameter, a density-

weighted injection velocity, defined in (19). For all fuel-injection velocities, the analysis reveals significant differences between the potential-flow solution, which involves a nonzero tangential velocity component on the surface of the porous cylinder, and the solution with fuel injection normal to the cylinder surface, likely prevailing in most applications of this type. In the limit of small injection velocities, for the latter (rotational) fuel-side flow, computations reveal early separation of a high-vorticity region from the vicinity of the cylinder, leading to the formation of a large wake, with the result that the rotational solution everywhere differs appreciably from that for potential fuel flow. In particular, in this limit of Λ approaching zero, the strain rate at the forward stagnation point approaches the classical value $2U_\infty/a$ for potential fuel flow but approaches only slightly more than 2/3 times that value when the fuel is injected normal to the cylinder surface. In general, with fuel injection normal to the cylinder surface, the streamline separating the fuel and air streams lies farther from the cylinder surface and experiences smaller strain rates. These results emphasize the importance of paying close attention to the fuel exit conditions in applying Tsuji burners in this manner to investigate diffusion-flame structures.

Acknowledgments

The authors of this paper are pleased to acknowledge the outstanding contributions of Paul Libby to combustion science. The two senior authors are grateful for many decades of enlightening scientific discussions with Paul (nearly six decades, in the case of FAW). Over the years, we greatly benefited from his profound understanding of the fluid mechanics involved in combustion processes and his ability to address key scientific problems using simple canonical flows. We hope that this contribution can serve as a small tribute in celebration of his life. We will always miss him.

Disclosure statement

No potential conflict of interest was reported by the author(s).

Funding

This work was supported by the National Science Foundation through grant # 1916979.

References

Batchelor, G. K. 2000. *An introduction to fluid dynamics*, 255–63. Cambridge (UK): Cambridge University Press.

Carpio, J., A. Liñán, A. L. Sánchez, and F. A. Williams. 2017. Aerodynamics of axisymmetric counterflowing jets. *Combust. Flame* 177:137. doi:10.1016/j.combustflame.2016.12.005.

Linán, A., and F. A. Williams. 1993a. *Fundamental aspects of combustion*, 61–73. New York, USA: Oxford University Press.

Linán, A., and F. A. Williams. 1993b. Ignition in an unsteady mixing layer subject to strain and variable pressure. *Combust. Flame* 95:31. doi:10.1016/0010-2180(93)90050-D.

Squires, N. Z., and P. A. Libby. 1994. Idealized two dimensional flames in premixed systems. *Combust. Sci. Tech* 103:21. doi:10.1080/00102209408907686.

Tsuji, H. 1982. Counterflow diffusion flames. *Prog. Ener. Combust. Sci* 8:93. doi:10.1016/0360-1285(82)90015-6.

Tsuji, H., and I. Yamaoka. 1967. The counterflow diffusion flame in the forward stagnation region of a porous cylinder. *Proc. Combust. Inst* 11:979. doi:10.1016/S0082-0784(67)80224-8.
Weiss, A. D., W. Coenen, and A. L. Sánchez. 2017. Aerodynamics of planar counterflowing jets. *J. Fluid Mech* 821:1. doi:10.1017/jfm.2017.192.
Williams, F. A. 1985. *Combustion Theory*, 10–11. Redwood City, CA: Addison-Wesley Publishing Co.
Zel'dovich, Y. B., A. G. Istratov, N. I. Kidin, and V. B. Librovich. 1980. Flame propagation in tubes: Hydrodynamics and stability. *Combust. Sci. Tech* 24:1. doi:10.1080/00102208008952419.

Appendix: The numerical scheme

The stream function is expressed in the form $\hat{\psi} = \hat{\psi}_p + \hat{\psi}_r$, where $\hat{\psi}_p$ is the potential-flow solution given by (20), and $\hat{\psi}_r$ is the rotational component, the latter determined by integration of

$$\frac{1}{r}\frac{\partial}{\partial r}\left(r\frac{\partial \hat{\psi}_r}{\partial r}\right) + \frac{1}{r^2}\frac{\partial^2 \hat{\psi}_r}{\partial \theta^2} = -\hat{\omega}(\hat{\psi}_p + \hat{\psi}_r). \tag{A1}$$

with boundary conditions

$$\begin{cases} \hat{\psi}_r = \partial\hat{\psi}_r/\partial r + 2\sin\theta = 0 & \text{at } r = 1 & \text{for } 0 \le \theta \le \pi \\ \hat{\psi}_r = 0 & \text{at } \theta = \pi & \text{for } 1 \le r < \infty \\ \hat{\psi}_r \to 0 & \text{as } r \to \infty & \text{for } 0 \le \theta \le \pi \\ \hat{\psi}_r = 0 & \text{at } \theta = 0 & \text{for } 1 \le r < \infty. \end{cases} \tag{A2}$$

The injection velocity Λ does not appear in the boundary conditions for $\hat{\psi}_r$; it enters only through $\hat{\psi}_p$, which may offer a simplification. The general strategy is to first guess a function $-\hat{\omega}(\theta)$ at $r = 1$ for $0 < \theta < \pi$, then solve the Poisson equation for $\hat{\psi}_r$ and calculate $\partial\hat{\psi}_r/\partial r$ at $r = 1$ for $0 < \theta < \pi$ to evaluate the difference Δ between that function and $-2\sin\theta$, on that boundary, which must vanish to satisfy the first boundary condition. The assumed function $-\hat{\omega}(\theta)$ is then increased by an amount proportional to this difference, and the solution process is repeated, again and again, until the difference Δ is less than at least 10^{-2}. Because of the dependence of the solution on Λ, a useful initial guess for $-\hat{\omega}(\theta)$ is $\sin\theta/(10\Lambda)$, and the increase at each step may best be taken to be the difference Δ divided by Λ; usually, only a small number (5 or 10) of iterations is needed, but that number increases substantially as Λ decreases below 0.1.

In the indicated procedure, the constancy of the vorticity along streamlines enables the source term in the Poisson equation to be evaluated throughout the field as a function of the stream function, but to solve the Poisson equation that source term must be known as a function of r and θ. That necessitates an inner sub-iteration in which, for each Poisson-equation solution, the stream function of the source term is evaluated as a function of r and θ from the previous solution. This sub-iteration should be continued until subsequent solutions throughout the field change by less than two significant figures, and in this work, it was continued until the change was less than 10^{-5}. Generally, a larger number of these sub-iterations is needed than the number of main iterations, and stability problems often were encountered, which were overcome by forcing the stream function of the source term to change by a sufficiently small amount from one iteration to the next, using in that source term a weighted mean of the current $\hat{\psi}_r$ and the previous $\hat{\psi}_r$. Occasionally, especially for large or small values of Λ, stability was achieved only when 90%, or even 99%, of the weight was ascribed to the previous $\hat{\psi}_r$. Convergence was, however, obtained in all cases.